Hindawi Publishing Corporation
Shock and Vibration
Volume 2015, Article ID 290714, 16 pages
http://dx.doi.org/10.1155/2015/290714

Research Article

Damage Detection and Quantification Using Transmissibility Coherence Analysis

Yun-Lai Zhou,[1] E. Figueiredo,[2] N. Maia,[3] and R. Perera[1]

[1]*Department of Mechanical Engineering, Technical University of Madrid, Jose Gutierrez Abascal 2, 28006 Madrid, Spain*
[2]*Faculdade de Engenharia da Universidade Lusófona, Campo Grande 376, 1749-024 Lisbon, Portugal*
[3]*LAETA, IDMEC, Instituto Superior Técnico, University of Lisbon, Avenida Rovisco Pais, 1049-001 Lisbon, Portugal*

Correspondence should be addressed to Yun-Lai Zhou; yunlai.zhou@alumnos.upm.es and R. Perera; ricardo.perera@upm.es

Received 23 November 2014; Revised 10 March 2015; Accepted 15 March 2015

Academic Editor: Peng Chen

A new transmissibility-based damage detection and quantification approach is proposed. Based on the operational modal analysis, the transmissibility is extracted from system responses and transmissibility coherence is defined and analyzed. Afterwards, a sensitive-damage indicator is defined in order to detect and identify the severity of damage and compared with an indicator developed by other authors. The proposed approach is validated on data from a physics-based numerical model as well as experimental data from a three-story aluminum frame structure. For both numerical simulation and experiment the results of the new indicator reveal a better performance than coherence measure proposed in Rizos et al., 2008, Rizos et al., 2002, Fassois and Sakellariou, 2007, especially when nonlinearity occurs, which might be further used in real engineering. The main contribution of this study is the construction of the relation between transmissibility coherence and frequency response function coherence and the construction of an effective indicator based on the transmissibility modal assurance criteria for damage (especially for minor nonlinearity) detection as well as quantification.

1. Introduction

Structural health monitoring (SHM) has experienced a huge development from more than four decades ago since the rehabilitation cost of oil pipes, bridges, tall buildings, and so on rapidly increased. In the last two decades, a lot of SHM methods have been developed based on both physics and data models. For instance, one systematic SHM solution for bridge maintenance is presented in [1], where both kinds of models are combined to identify damage. Other SHM solutions can be found in [2, 3].

For large and complex structures the use of accelerometers has made possible the development of vibration-based methods to analyze structures. Modal testing is the most common; by carrying out the experimental modal analysis (EMA) of a structure, some modal parameters, such as frequency, mass, and damping, can be extracted and a frequency response function (FRF) can be obtained. This will make possible the construction of different damage indicators. Modal testing is also conducted on structures in real operational conditions, within which the excitation will be very difficult or even impossible to be measured; operational modal analysis (OMA) uses the response signals only to extract the structural dynamic parameters in order to assess the structural states. In addition, for long-term operating structures, like oil pipes, turbines, or bridges, statistical methods are also developed for real-time online SHM systems.

In real engineering, motivated on solving the difficulty in capturing the excitation, in the middle of 1980s, transmissibility (or direct transmissibility) was raised. Instead of considering the input and output signals of the structural system, transmissibility only pays attention to the outputs; that is, it concentrates on the interrelation of two outputs of the structure, in order to create a connection with the structural dynamic characteristic. Afterwards, a lot of researchers developed it for parameter identification [4], damage detection as well as quantification [5], uncertainty analysis [6], and response/excitation (i.e., force) reconstruction [7], and so on. In [4], relative mode shape is extracted

from the transmissibility in the natural resonant frequencies, which avoids the use of FRF in mode shape estimation. In [5], a method of taking advantage of response vector assurance criterion (RVAC) [8] was proposed, replacing the FRF by transmissibility function in the indicator RVAC, and detection and relative damage quantification indicator (DRQ) [9], which is the average value of RVAC along the frequency domain. The RVAC is a simplified form of FDAC, which was defined by Heylen et al. [8]. The key idea is to use the sum of all coordinates FRF before and after damage of all loading conditions in the form of modal assurance criteria.

However, the detection of damage, at an early stage, is still a very difficult and challenging task; therefore, the proposal of new indicators based on dynamic responses that may be sensitive enough to minor damage is very important. In this sense, the coherence, as a function dependent on the frequency and able to analyze the spatial correlation between two signals [10, 11] might be potentially a good starting point to develop sensitive damage indicators.

The coherence function, formally defined by Wiener [12, 13], has been extensively studied and used, especially after the development of the Fourier transform, in a lot of research fields, with extensions to the most modern wavelet coherence and partial directed coherence: neurology, mostly in electroencephalography (EEG) studies [14–16], like EEG microstates detection in insight and calm meditation [14]. Coherence is also used in skin blood oscillations analysis in human [17], nerve fiber layer thickness quantification [18].

In another aspect, spatial coherence measure is also developed for signal enhancement [19] by designing coherence-based post filters. In recent years, coherence function has been used in mechanical engineering for damage identification, namely, detection, type, and quantification [20–24]. In [20], a coherence algorithm is proposed for damage type recognition and damage localization for large flexible structures with a nine-bay truss example; the key idea is to construct a connection between coherence and transfer function, and the transfer function parameter change is extracted for damage detection. In [21], local temporal coherence is developed and extended to time-varying process with the basic coherence conception from the cross correlation defined in [25], and the corresponding peak value is defined as peak coherence, creating a connection with the temperature and introduced damage change; that is, the peak coherence for temperature/damage change is somewhat a function of time. In addition, the peak performs well in distinguishing environmental change and damage. In [22, 23], coherence is integrated in the frequency domain and set as an indicator-coherence measure, as a sensitive enough indicator for quantifying the skin damage and assessing restoration quality. In [24], coherence measure based method, as a time series method, is developed for fault detection and identification in vibrating structures.

In this paper, coherence analysis of transmissibility is performed, and from it an effective indicator for damage, especially nonlinearity, is proposed and compared with the coherence measure raised in [22]. In order to test the feasibility of the proposed approach, numerical simulation of a laboratory structure is carried out, and, additionally, experimental measurements on a three-story aluminum structure are used to check the applicability of the proposed indicator.

2. Transmissibility Based Coherence

As described in [2], SHM is essentially a statistical pattern recognition problem. It can be described as a four-stage process:

(1) operational evaluation,

(2) data acquisition, Fusion, and Cleansing,

(3) feature extraction and information condensation,

(4) statistical model development for feature discrimination.

As for vibration-based SHM, the core idea is to find a sensitive feature able to discriminate a damaged structure when compared to the baseline structure (healthy state); therefore the damage detection conclusion can be drawn out with choosing a threshold of the change, before and after damage, considering the influence of operational variety. As described in the introduction, lots of approaches, features, and measurement methodologies have been used in the past [2, 3, 26, 27].

2.1. Applicability of Coherence in Damage Detection. As commented in the introduction, coherence has been used in many applications. It is useful to examine the correlation between two frequency signals, in a similar way to the correlation coefficient in frequency. More details can be found in [28].

Coherence, as a complex measure, is estimated by dividing the square of the cross-spectral density between two signals by the product of the autospectral densities of both signals. Consequently, it will be sensitive to both changes in power and phase relationships in one of the two signals [29].

The magnitude-squared coherence for the bivariate time series enables us to identify significant frequency-domain correlation between the two time series [30]. For the purpose of preventing obtaining an estimate of magnitude-squared coherence to be identically 1 for all frequencies, an averaged magnitude-squared coherence estimator has to be used. Both Welch's overlapped segment averaging (WOSA) and multitaper techniques are appropriate [30]. In this study, WOSA is utilized for the coherence estimate. A detailed discussion of several seemingly disparate nonparametric magnitude squared coherence estimation methods including Welch's averaged periodogram, the minimum variance distortionless response (MVDR), and the canonical correlation analysis (CCA) can be found in [31].

For SHM purposes, the most important task is to find a structural feature sensitive to the occurrence of damage. Methodologies involving coherence have been developed in the past decades [20–24, 32]. As proved in [22–24], a coherence based damage indicator can be used in damage detection. The premise behind this is that the coherence will decrease as nonlinearity increases.

2.2. Transmissibility. Considering a linear multiple-degree-of-freedom system, the dynamic equilibrium equation can be written by the well-known second order differential equation:

$$M\ddot{x}(t) + C\dot{x}(t) + Kx(t) = f(t), \tag{1}$$

where M, C, and K are the mass, damping, and stiffness matrices of the system, respectively, $f(t)$ is the input force vector, and $x(t)$ contains the responses of each degree-of-freedom of the system.

Herein, for a harmonic applied force at a given coordinate, the transmissibility between point i and a reference point j can be defined as

$$T_{(i,j)} = \frac{X_i(\omega)}{X_j(\omega)}, \tag{2}$$

where X_i and X_j are the complex amplitudes of the system responses $x_i(t)$ and $x_j(t)$, respectively, and ω is the frequency [4].

In order to calculate the transmissibility, no matter in real engineering or experiment analysis, apart from direct extracting from the two responses, it can be derived in several ways [5]; for instance, using the FRFs,

$$T_{(i,j)} = \frac{X_i(\omega)/F_l(\omega)}{X_j(\omega)/F_l(\omega)} = \frac{H_{(i,l)}(\omega)}{H_{(j,l)}(\omega)}, \tag{3}$$

where l is the excitation point and H represents the FRF. Note that herein the transmissibility is a norm that estimates the structural dynamic responses.

2.3. Transmissibility Coherence. Given the structural system described above with one single excitation, the FRF of points i to l can be calculated by two forms in estimation; that is,

$$\begin{aligned} H_1(\omega) &= \frac{S_{(i,l)}(\omega)}{S_{(l,l)}(\omega)}, \\ H_2(\omega) &= \frac{S_{(i,i)}(\omega)}{S_{(l,i)}(\omega)}, \end{aligned} \tag{4}$$

where S represents the auto- and cross-spectrum for the two points. Correspondingly, the coherence function (or magnitude squared coherence function) is indicated as [33, 34]

$$\begin{aligned} \gamma^2 = \frac{H_1(\omega)}{H_2(\omega)} &= \frac{S_{(i,l)}(\omega)}{S_{(l,l)}(\omega)}\frac{S_{(l,i)}(\omega)}{S_{(i,i)}(\omega)} \\ &= \frac{S_{(i,l)}(\omega)}{S_{(i,i)}(\omega)}\frac{S^*_{(i,l)}(\omega)}{S_{(l,l)}(\omega)} = \frac{\left|S_{(i,l)}(\omega)\right|^2}{S_{(i,i)}(\omega)S_{(l,l)}(\omega)}. \end{aligned} \tag{5}$$

By analogy with (5), the transmissibility coherence (TC) can be defined from (3) as follows:

$$\begin{aligned} \gamma^2_{\mathrm{TC}} = \frac{T_{1(i,j)}(\omega)}{T_{2(i,j)}(\omega)} &= \frac{H_{1(i,l)}(\omega)/H_{1(j,l)}(\omega)}{H_{2(i,l)}(\omega)/H_{2(j,l)}(\omega)} \\ &= \frac{H_{1(i,l)}(\omega)}{H_{2(i,l)}(\omega)}\frac{H_{2(j,l)}(\omega)}{H_{1(j,l)}(\omega)} = \frac{\gamma^2_{(i,l)}}{\gamma^2_{(j,l)}}. \end{aligned} \tag{6}$$

Herein, above all, transmissibility coherence means the magnitude squared coherence; secondly, from the equation above, one can see that the TC can be calculated directly from the coherence of corresponding FRFs, which gives a way for estimating the transmissibility coherence in laboratory experiments analysis. Thirdly, note that herein the TC, as an estimation indicator for transmissibility, that is, coherence for two outputs, is an indicator revealing the coherence/correlation between two outputs with considering the excitation point.

On the other hand, if direct transmissibility is directly estimated using two outputs, that is, not taking the FRFs into account, referring to the conception of coherence [12, 13, 34], TC can be also derived solely by using the auto- and cross-spectrum of the two responses signals:

$$\begin{aligned} T_{1(i,j)} &= \frac{X_i(\omega)}{X_j(\omega)}\frac{X_j(\omega)}{X_j(\omega)} = \frac{S_{(i,j)}(\omega)}{S_{(j,j)}(\omega)}, \\ T_{2(i,j)} &= \frac{X_i(\omega)}{X_j(\omega)}\frac{X_i(\omega)}{X_i(\omega)} = \frac{S_{(i,i)}(\omega)}{S_{(j,i)}(\omega)}. \end{aligned} \tag{7}$$

From (7), TC will be exp as

$$\begin{aligned} \gamma^2_{\mathrm{TC}} = \frac{T_{1(i,j)}(\omega)}{T_{2(i,j)}(\omega)} &= \frac{S_{(i,j)}(\omega)/S_{(j,j)}(\omega)}{S_{(i,i)}(\omega)/S_{(j,i)}(\omega)} \\ &= \frac{S_{(i,j)}(\omega)S_{(j,i)}(\omega)}{S_{(j,j)}(\omega)S_{(i,i)}(\omega)} = \frac{\left|S_{(i,j)}(\omega)\right|^2}{S_{(i,i)}(\omega)S_{(j,j)}(\omega)}. \end{aligned} \tag{8}$$

Fourier transform in (8) gives the frequency distribution of TC. For the TC estimation, Welch method [35] and minimum variance distortionless response (MVDR) [36] method are commonly used.

As the coherence is a squared magnitude, TC is higher than zero. Comparing (6) and (8), one can observe that TC can be estimated in two ways: from the coherence of FRF like in (6) and from direct estimation, as described in (8). Similar to FRF coherence, the first function of TC is for checking whether the experiment is well conducted. And basically, TC reveals the coherence of two outputs; that is, it indicates the interrelation of the dynamic characteristics of two outputs. Therefore, it is assumed that when the damage occurs in a structure, TC, as a sensitive indicator, will change compared to the baseline of the structural system, and so it might be used to detect structural damage.

3. Damage Identification Based on TC

3.1. Damage Indicators. By using a similar approach to [22–24], a TC damage indicator is defined here based on the accumulation of TC along frequency domain as follows:

$$\mathrm{ATC} = \int_{f_{\min}}^{f_{\max}} \mathrm{TC}\,df, \tag{9}$$

where the interval $[f_{\min}, f_{\max}]$ is the frequency bandwidth of interest for our problem. As TC $>$ 0, then ATC $>$ 0.

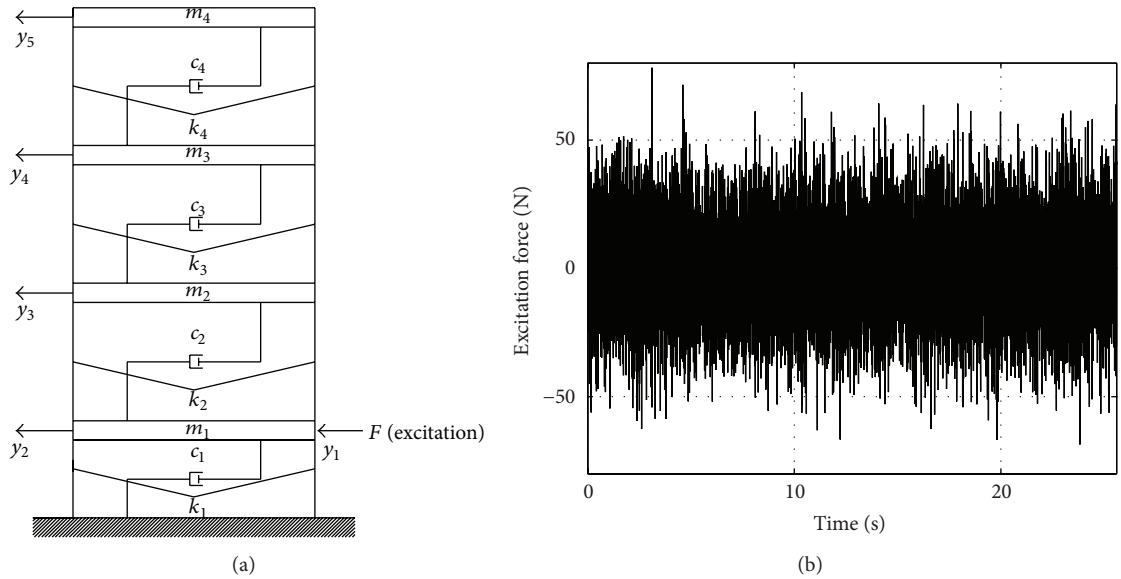

Figure 1: (a) Shear-building model of a three-story structure. (b) The excitation force.

Compared to the coherence measure in [22], the basic idea is the same, being the main difference that ATC is computed from the coherence between two output responses instead of excitation-response.

Additionally, another indicator has been defined based on the MAC criterion [37–40]. For its application, a vector is defined grouping the values of TC for each spectrum line. Considering the same dimension for each TC set, a transmissibility modal assurance criterion (TMAC) is defined as follows:

$$\text{TMAC} = \frac{\left|\left(\left(\text{TC}(w)\right)^{d}\right)^{T}\left(\text{TC}(w)\right)^{u}\right|^{2}}{\left(\left(\left(\text{TC}(w)\right)^{d}\right)^{T}\left(\text{TC}(w)\right)^{d}\right)\left(\left(\left(\text{TC}(w)\right)^{u}\right)^{T}\left(\text{TC}(w)\right)^{u}\right)}, \tag{10}$$

where $(\,)^{d}$ means the vector under damage scenario, $(\,)^{u}$ means the vector under healthy condition, and $(\,)^{T}$ means the transposed form of the vector.

Theoretically speaking, for each damage scenario, TMAC $\in [0, 1]$. If the TMAC is "1," the structure is totally undamaged; if the TMAC is very close to "1," it means that the structure is confidently undamaged; and when the TMAC value decreases, it means that damage or deterioration is occurring in the structure; as the TMAC gets close to "0," it means that the damage severity increased. Finally, if the TMAC is "0," the structure is severely damaged.

In conclusion, two different damage indicators based on TC have been proposed to detect structural damage. The damage quantification indicators ATC and TMAC intend to extract a global indicator, which might be monotonically related to the structural damage. Basically, the indicator increases as the severity of damage or nonlinearity increases. Due to this fundamental idea, the ATC performs by accumulating all the coherence value to each measurement of damage scenarios, which will reveal the whole interrelation of the two outputs. The TMAC performs using the assurance criterion principals.

3.2. Damage Identification Scheme. Damage identification scheme will be conducted as follows.

Step 1 (response measurement). In this step, the vibration dynamic responses of the studied structure will be captured.

Step 2 (transmissibility extraction). In this step, transmissibility will be estimated via (3).

Step 3 (coherence estimation). Coherence will be estimated, and we determine whether the experiment is well conducted; if not, Step 1 will be redone for a new measurement.

Step 4 (damage feature calculation). Regarding the estimated coherence from Step 3, damage sensitive features are calculated and analyzed for detecting the potential damage.

4. Numerical Simulation

4.1. Model Description. For the purpose of evaluating the feasibility of the proposed approach, a physics-based numerical model is developed. The test structure is modeled as four-lumped masses at the floors, including the base that slides on rails, as shown in Figure 1(a). The excitation point is at the base as shown in Figure 1(a); the responses ("y_1," "y_2," "y_3," "y_4," and "y_5") are measured at each floor. Figure 1(b) shows a sample from a random excitation [40].

In this case, damage is introduced by increasing the mass at the base and first floor as well as stiffness reduction at the columns, as listed in Table 1. Random noise is

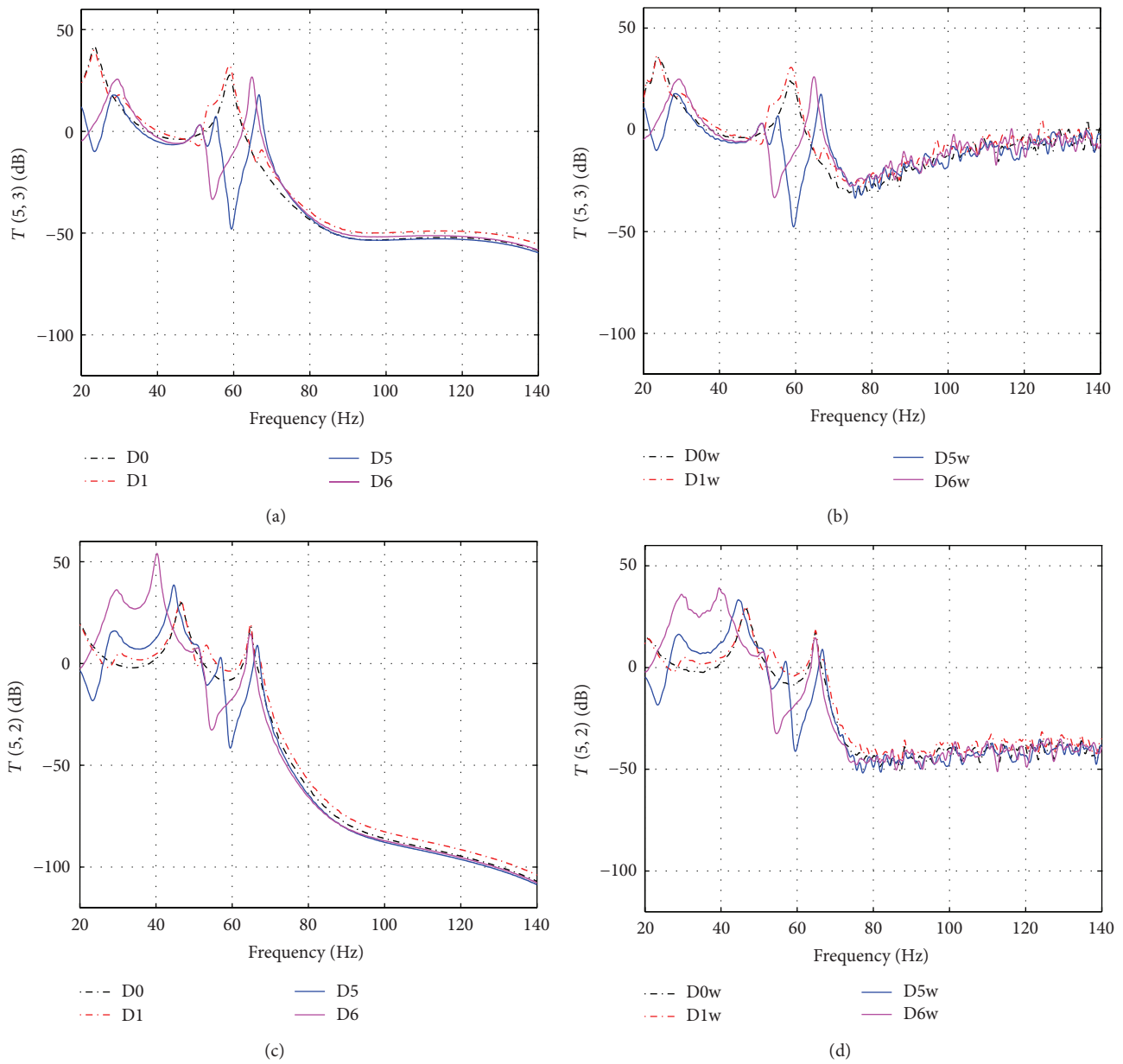

FIGURE 2: T (5, 3) and T (5, 2) for damage scenarios D0, D1, D5, and D6: (a) without random noise, (b) with 5% random noise, (c) without random noise, and (d) with 5% random noise.

introduced to the system for comparison in analysis. The 87.5% reduction in stiffness was chosen in order to be consistent with the experimental procedure developed in [40].

4.2. Transmissibility, TC, and FRF Coherence Comparison

4.2.1. Transmissibility and TC Comparison. Considering the personal experience in transmissibility work, one can choose transmissibility between different nodes; however, results might be quite different. And, therefore, to choose transmissibility is a difficult mission, which will greatly influence the potential results. Here, in this study of the simple structure, all the transmissibilities can be plotted and later analyzed; however, not all the transmissibilities will perform very well. Some representative transmissibilities and related indicators are analyzed in this study according to the engineer experience. Figures 2(a) and 2(b) show the transmissibility between nodes 5 and 3 and 5 and 2, T (5, 3) and T (5, 2), for damage scenarios D0, D1, D5, and D6 without and with 5% random noise, respectively. From all Figures 2(a)–2(d), little difference between D0 and D1 can be observed, which suggests that "adding 1.2 Kg to the base" has very small effect to the dynamic responses. From Figures 2(a) and 2(c), one can observe small differences in the second half of the frequency domain, and two peak shifts can be found in the first half of the frequency domain, which might be used for predicting damage.

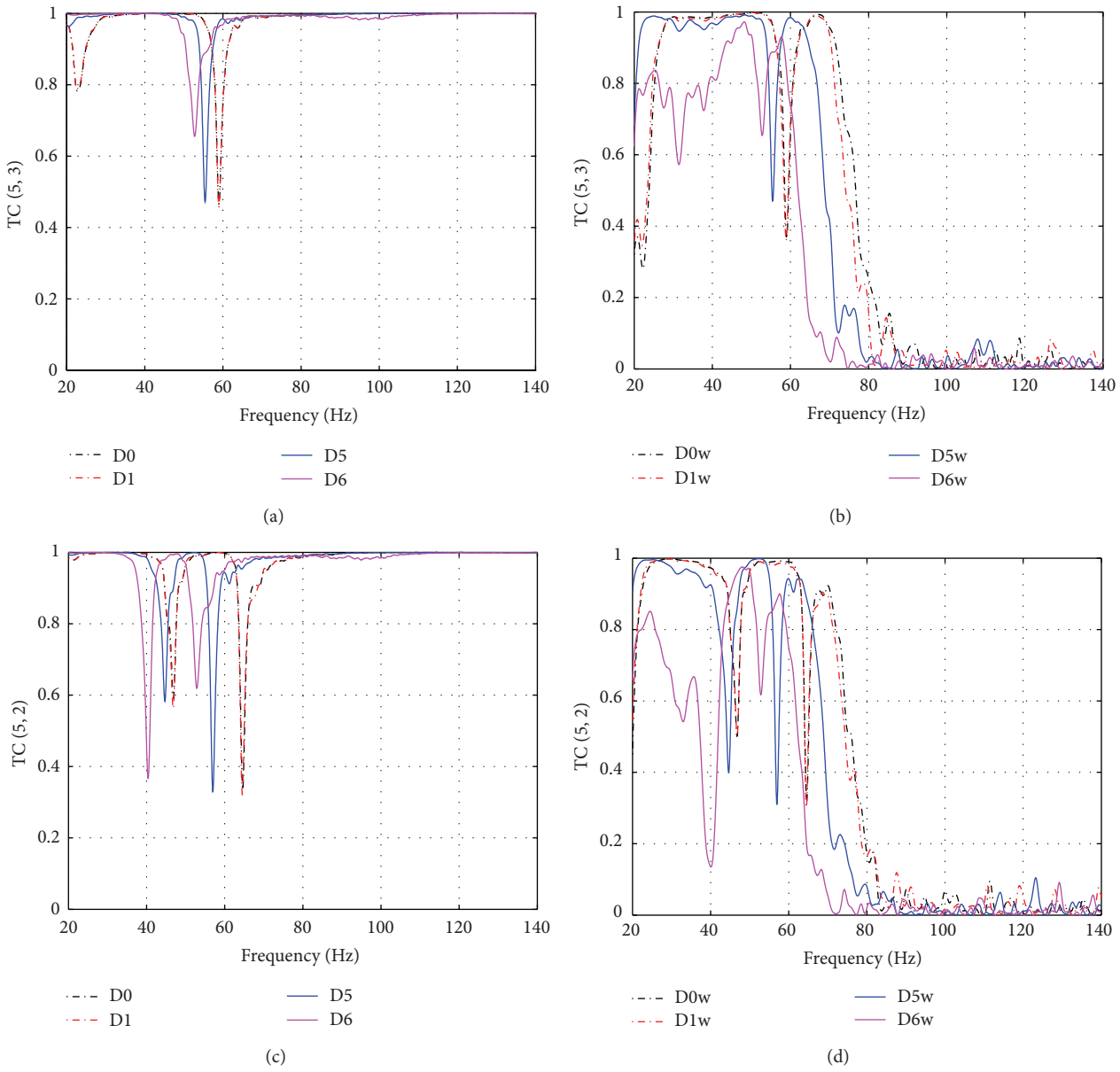

Figure 3: TC (5, 3) and TC (5, 2) for damage scenarios D0, D1, D5, and D6: (a) without random noise, (b) with 5% random noise, (c) without random noise, and (d) with 5% random noise.

Table 1: Damage scenario.

Damage scenario	Case description
D0	Baseline (undamaged condition)
D1	Add mass 1.2 kg at the base
D2	Add mass 1.2 kg at the first floor
D3	50% stiffness reduction in $k2$
D4	87.5% stiffness reduction in $k2$
D5	50% stiffness reduction in $k3$
D6	87.5% stiffness reduction in $k3$
D7	50% stiffness reduction in $k4$
D8	87.5% stiffness reduction in $k4$

In Figures 2(b) and 2(d), it is clear that the random noise introduced some influence into the transmissibility, especially visible in the high frequency domain (>80 Hz), which is heavily affected by the noise. Furthermore, comparing Figures 2(c) and 2(d), it can be observed that the peak value of D6w at 40 Hz was reduced by the random noise effect, which might add challenge in the process of damage detection.

Figures 3(a), 3(b), 3(c), and 3(d) plot the transmissibility coherence, TC (5, 3) and TC (5, 2), for damage scenarios D0, D1, D5, and D6 without and with 5% random noise, respectively. The TC (5, 3) and TC (5, 2) overlap in all the frequencies to the case without random noise and overlap in most of the frequencies to the case with 5% random noise between D0 and D1. This confirms the conclusion in

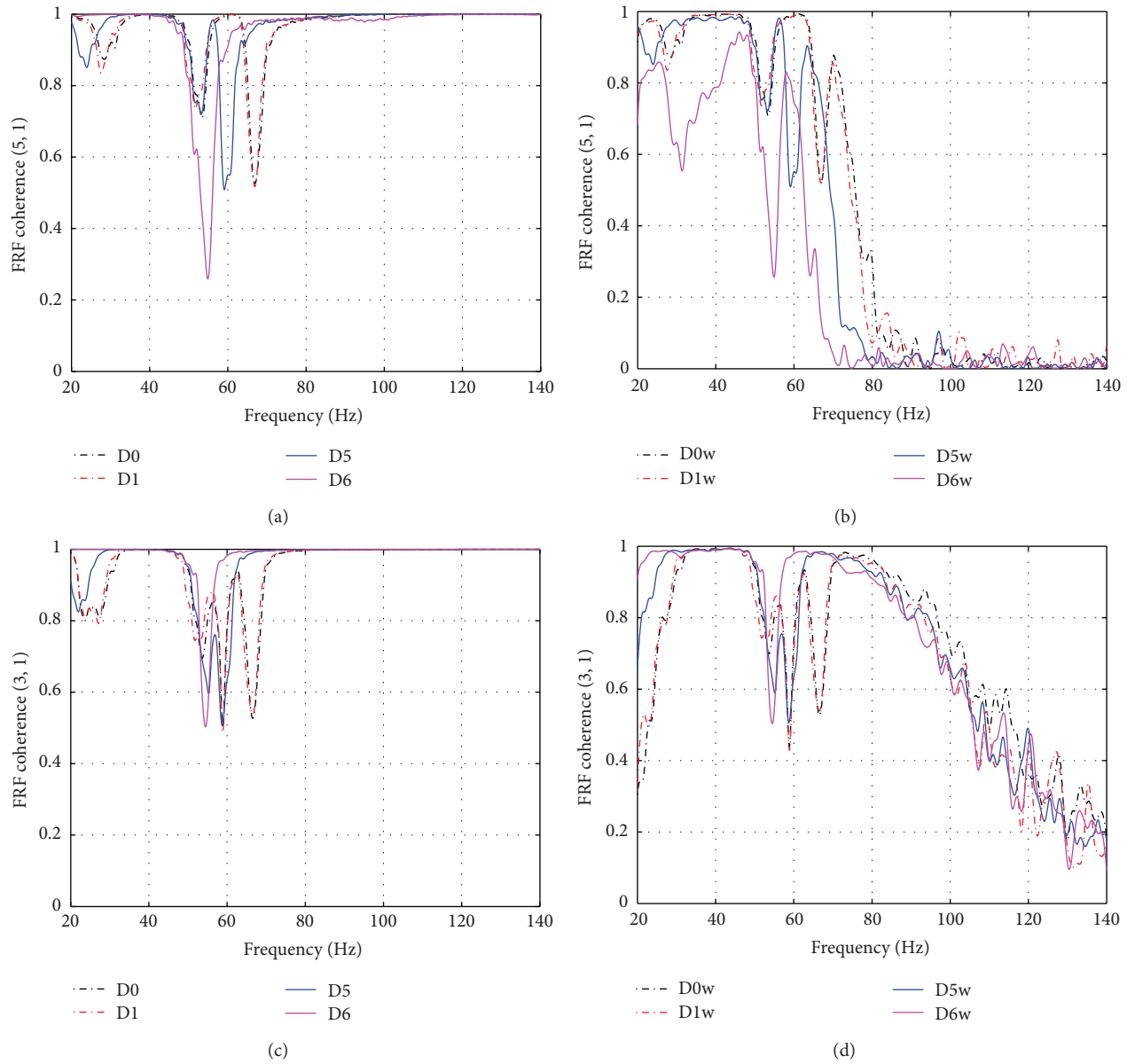

Figure 4: FRF coherence (5, 1) and FRF coherence (3, 1) for damage scenarios D0, D1, D5, and D6: (a) without random noise, (b) with 5% random noise, (c) without random noise, and (d) with 5% random noise.

the aforementioned discussion in T (5, 3) and T (5, 2) that "adding 1.2 Kg to the base" contributes little to the dynamic responses.

From Figures 3(a) and 3(c), one can find that TC (5, 2) has two peaks for each scenario while TC (5, 3) only has one peak for D5 and D6, while it has two peaks for D0 and D1. Then, from D0 to D5 and D6, the peaks shift toward left side; that is, the corresponding frequencies decrease. The same pattern can be observed in Figures 3(b) and 3(d), when the data are smeared with noise. As TC is for estimating the two outputs of a structural system, change will be introduced to the dynamic outputs when damage occurs, which will later cause effect to TC, like frequency shift. And therefore, from this aspect, TC might be used to detect damage.

From Figures 3(b) and 3(d), another phenomenon can be observed, as noise influences a lot the TC; this might be used to check whether the experiment is well conducted, which shares the same function of FRF coherence in real engineering but has more potentiality as excitation not always can be measured. If the experiment is well conducted without being highly influenced by the environmental variety like noise, then nonlinearity occurrence or novelty existence might be taken into account.

4.2.2. TC and FRF Coherence Comparison. For the purpose of comparing with TC discussed above, and due to the reason that TC is for two outputs, and FRF coherence is for the one input and one output, herein some representative FRF coherences are selected according to the engineer experience. Figures 4(a), 4(b), 4(c), and 4(d) show the FRF coherence (5, 1) and FRF coherence (3, 1) without and with 5% random noise, respectively.

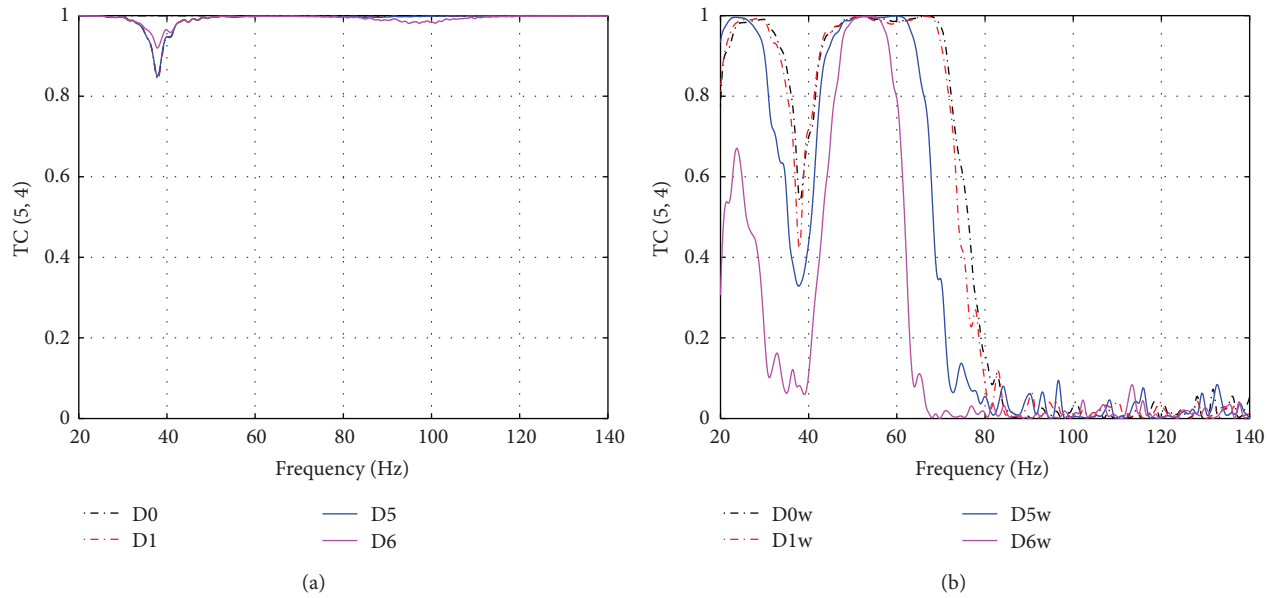

Figure 5: TC (3, 2) for damage scenarios D0, D5, and D6: (a) without noise and (b) with 5% random noise.

To the mass influence, from Figures 4(a) and 4(c), one can find that the difference between D0 and D1 is very little, which confirms the analysis before in T and TC.

To the stiffness reduction influence, to the without-noise cases, that is, in Figures 4(a) and 4(c), it can be also found that peak frequency shifts from D0 to D5 and D6; that is, the peak frequency difference before and after damage is clear, which suggests that it might be used as damage-sensitive feature. On the other hand, in the case with random noise, Figures 4(b) and 4(d) show that the differences are apparently higher for the FRF coherence (5, 1) than FRF coherence (3, 1). Thus, it indicates that if the FRF coherence is not well chosen, then it might be hard to detect damage.

Additionally, one can also notice that noise highly affects the coherence in the high frequency domain, which inputs higher power of noise in that frequency domain. In real situations, the result presented in Figures 4(b) and 4(d) suggests that the experiment is badly conducted and it should be reconducted, as normally 0.9 is the threshold for coherence analysis. And if in the frequency band of interest lots of values are lower than 0.9, it means that the experiment might be wrongly done or badly influenced by noise. If the experiment is well conducted, it might mean that nonlinearity occurs or novelty happens. This conclusion is similar to the discussion of TC aforementioned.

With regard to Figure 4(d), and from Figure 5, one can find that if the TC is not well chosen, it will be also challenging in detecting with the frequency shift, like in Figures 5(a) and 5(b). This also confirms the same idea of FRF coherence discussed above.

Finally, from the discussion above, one might conclude the following.

(a) The comparison between Figures 3 and 4 indicates that both the FRF coherence and the TC have the ability to unveil differences when damage is present in the structure if they are well chosen.

(b) "Adding 1.2 Kg" to the base did quite little influence to the dynamic responses according to the T, TC, and FRF coherence analysis.

(c) For both TC and FRF coherence, peak shifts might be used for detecting damage, as the TC (5, 3) and TC (5, 2) and FRF coherence (5, 1) perform well in differentiating the damage cases from the baseline. However, if TC and FRF coherence are not well chosen, it will be challenging in detecting damage via the peak frequency shift.

(d) As TC has the same ability, as FRF coherence, in checking whether the experiment is well conducted, then its output-only characteristic might be considered better than FRF coherence in the data acquisition aspect, as the excitation in real engineering is not always possible to be measured.

4.3. Damage Identification Procedure. For the indicators described in Section 3.1, herein, Table 2 summarizes the ATC (5, 3) from damage scenarios D0 to D8 without and with 5% random noise.

For the case with adding mass to the base or the first floor, from Table 2, from D0 to D1 and D2, it can be observed that ATC (5, 3) decreases as the mass is added into the base and decreases continually as the mass is moved from the base to the first floor in all the cases without noise and with random noise.

For the case of stiffness reduction, from Table 2, one can observe that ATC (5, 3) does not hold the same rule; from D4 to D8, to all the integration types, values more than "1" exist; that is, it will be challenging in drawing out a conclusion for detecting damage, or it is hard to find a clear rule for predicting damage. This means that ATC might not work in linear part. The discussion about ATC in nonlinearity part will be addressed in the later experiment result discussion.

Table 2: ATC (5, 3) for damage scenarios D0 to D8.

Damage scenario	ATC (5, 3)							
	[0, 80] (Hz)		[20, 80] (Hz)		[40, 80] (Hz)		[40, 140] (Hz)	
	Noise free	5% noise	Noise free	5% noise	Noise free	5% noise	Noise free	5% noise
D0	1.0000	1.0000	1.0000	1.0000	1.0000	1.0000	1.0000	1.0000
D1	**0.9989**	**0.9802**	**1.0000**	**0.9807**	**0.9994**	**0.9627**	**0.9998**	**0.9491**
D2	**0.9990**	**0.9613**	**0.9993**	**0.9643**	**0.9986**	**0.9474**	**0.9995**	**0.9322**
D3	0.9927	0.9204	0.9995	0.9026	0.9976	0.8334	0.9993	0.8192
D4	*1.0159*	*0.7384*	*1.0081*	*0.7091*	*1.0058*	*0.5854*	*1.0026*	*0.5798*
D5	0.9739	0.9287	1.0149	0.9431	1.0027	0.8124	1.0010	0.7998
D6	0.9888	0.7313	1.0134	0.7024	0.9975	0.6208	0.9959	0.6172
D7	0.9716	0.9274	1.0052	0.9255	0.9989	0.8487	0.9998	0.8373
D8	0.9959	0.8350	1.0102	0.8248	1.0069	0.6853	1.0030	0.6872

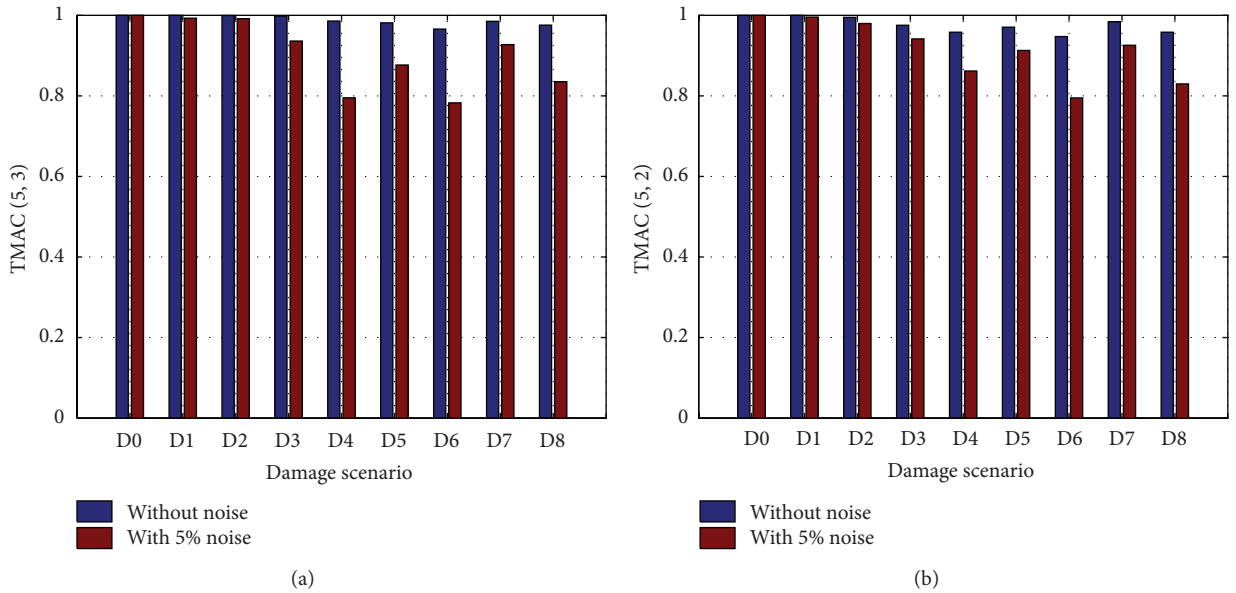

Figure 6: (a) TMAC (5, 3) for damage scenarios D0–D8; (b) TMAC (5, 2) for damage scenarios D0–D8.

Finally, TMAC (5, 3) and TMAC (5, 2) are plotted in Figures 6(a) and 6(b), respectively. For the mass adding type, from D0 to D1 and D2, one can observe that in both TMAC (5, 3) and TMAC (5, 2), the TMAC varies insignificantly, which need to be identified by graphical amplification. For the stiffness reduction type, the TMAC (5, 3) and TMAC (5, 2) vary clearly for each column stiffness reduction, like from D3 to D4, from D5 to D6, and from D7 to D8, respectively. In conclusion, these observations suggest that TMAC might be used for relative damage quantification.

5. Experimental Verification

For testing the applicability of the proposed methodology in complex structures, a three-story building structure [41] testing data from the Los Alamos National Laboratory is used. As shown in Figure 7, for each floor, four aluminum columns ($17.7 \times 2.5 \times 0.6\ \text{cm}^3$) are connected with the top and bottom aluminum plates ($30.5 \times 30.5 \times 2.5\ \text{cm}^3$). The structure performs as a four-degree-of-freedom (DOF) system. Bolt joints are used to assemble each connection between columns and plates. In addition the structure slides on rails that allow movement only in the x-direction. A center column ($15.0 \times 2.5 \times 2.5\ \text{cm}^3$) is suspended from the top floor. This column is used as a source of damage that induces nonlinear behavior when it contacts a bumper mounted on the next floor. The position of the bumper can be adjusted to vary the extent of impacting that occurs during a particular excitation level.

An electrodynamic shaker provides a lateral excitation to the base floor along the centerline of the structure. The structure and shaker are mounted together on an aluminum base plate ($76.2 \times 30.5 \times 2.5\ \text{cm}^3$) and the entire system rests on rigid foam. The foam is intended to minimize extraneous sources of unmeasured excitation from being introduced through the base of the system. A load cell (Channel 1) was attached at the end of a stinger to measure the input force from the shaker to the structure. Four accelerometers (Channels 2–5) with nominal sensitivities of 1000 mV/g were attached at the centerline of each floor on the opposite side from the excitation source to measure the system response.

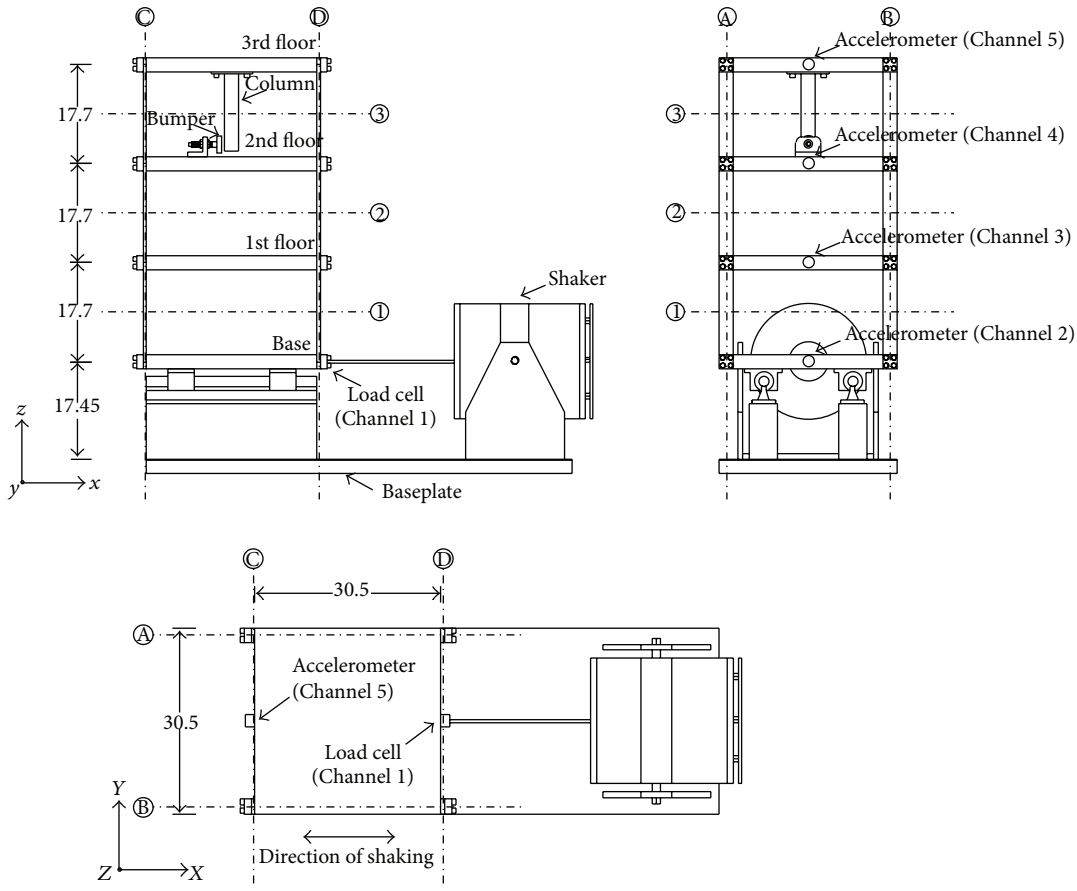

Figure 7: Schematic representation of the three-story building structure (all dimensions are in cm).

Table 3: Structural state condition.

Label	State condition	Case description
State #1	Undamaged	Baseline condition
State #2	Undamaged	Added mass (1.2 Kg) at the base
State #3	Undamaged	Added mass (1.2 Kg) at the first floor
State #4	Undamaged	Stiffness reduction in column 1BD
State #5	Undamaged	Stiffness reduction in columns 1AD and 1BD
State #6	Undamaged	Stiffness reduction in column 2BD
State #7	Undamaged	Stiffness reduction in columns 2AD and 2 BD
State #8	Undamaged	Stiffness reduction in column 3BD
State #9	Undamaged	Stiffness reduction in columns 3 AD and 3 BD
State #10	Damaged	Gap (0.2 mm)
State #11	Damaged	Gap (0.15 mm)
State #12	Damaged	Gap (0.13 mm)
State #13	Damaged	Gap (0.10 mm)
State #14	Damaged	Gap (0.05 mm)
State #15	Damaged	Gap (0.2 mm) and mass (1.2 Kg) at the base
State #16	Damaged	Gap (0.2 mm) and mass (1.2 Kg) on the 1st floor
State #17	Damaged	Gap (0.1 mm) and mass (1.2 Kg) on the 1st floor

Force and acceleration time-series from 17 different structural state conditions were collected as given in Table 3. For instance, "State #4" is described as "stiffness reduction in column 1BD," which means that there was an 87.5% stiffness reduction (corresponding to a 50% reduction in the column thickness) in the column located between the base and first floor at the intersection of planes B and D. For each structural state condition, data were acquired from 50 separate tests.

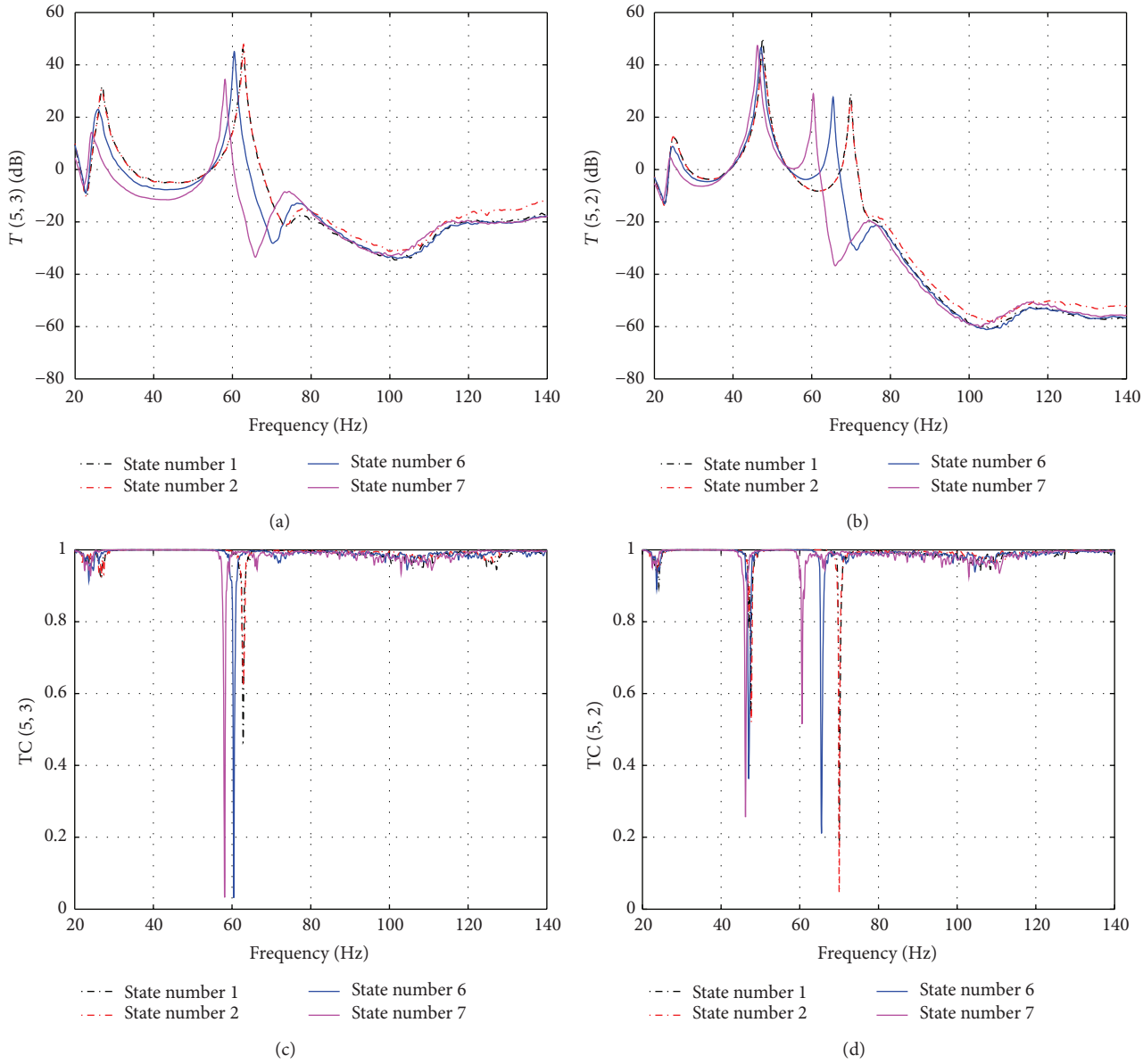

Figure 8: (a) T (5, 3), (b) T (5, 2), (c) TC (5, 3), and (d) TC (5, 2) of measurement 1 of State numbers 1, 2, 6, and 7.

For each test, the data correspond to a set of five time series measured with the input force transducer and the four accelerometers.

The structural state conditions can be categorized into four main groups. The first group is the baseline condition. The baseline condition is the reference structural state and is labeled "State #1" in Table 3. The bumper and the suspended column are included in the baseline condition, but the spacing between them was maintained in such a way that there were no impacts during the excitation. The second group includes the states with simulated operational and environmental variability. Such variability often manifests itself in changes in the stiffness or mass distribution of the structure. In order to simulate such operational and environmental condition changes, tests were performed with different mass-loading and stiffness conditions (State numbers 2–9). The mass changes consisted of adding 1.2 kg (approximately 19% of the total mass of each floor) to the base and first floor. The stiffness changes were introduced by reducing the stiffness of one or more of the columns by 87.5%. This process was executed by replacing the corresponded column with one that had half the cross-sectional thickness in the direction of shaking.

Those changes were designed to introduce variability in the fundamental natural frequency up to, approximately, 7% from the baseline condition, which is within the range normally observed in real-world structures. More details about the test structure as well as data sets can be found in Figueiredo et al. [40, 41].

5.1. Transmissibility, TC, and FRF Coherence Comparison

5.1.1. Transmissibility and TC Comparison. In order to show the advantage of TC over transmissibility, a comparison

Table 4: The comparison of transmissibility, TC, and FRF coherence in peak change.

State	Indicator	Frequency shift (Hz)				Amplitude value			
		Peak 1	I (%)*	Peak 2	I (%)*	Peak 1	I (%)*	Peak 2	I (%)*
#1	T (5, 2)	47.54	—	69.92	—	50.18	—	28.95	—
#6		47.15	−0.82	65.47	−6.36	46.58	−7.17	27.62	−4.59
#7		46.25	−2.71	60.42	−13.59	47.42	−5.50	28.94	−0.03
#1	TC (5, 2)	47.58	—	70.08	—	0.54	—	0.18	—
#6		47.07	−1.07	65.55	−6.46	0.36	−33.33	0.21	0.17
#7		46.25	−2.80	60.63	−13.48	0.26	−51.85	0.52	188.89
#1	FRFC (5, 1)	54.88	—	71.88	—	0.83	—	0.80	—
#6		54.96	0.15	67.19	−6.52	0.76	−8.43	0.86	7.5
#7		54.69	−0.35	62.15	−13.54	0.78	−6.02	0.89	11.25

*Increase from the baseline "State #1."

between TC and transmissibility is proposed herein. Several representative TC and T have been chosen and studied according to the engineering experience. The extracted transmissibility, T (5, 3), T (5, 2), and transmissibility coherence, TC (5, 3), TC (5, 2), under State numbers 2, 6, and 7, along with baseline (State #1), are shown in Figure 8, which were calculated using the Welch based methods with Hanning window.

From Figures 8(a), 8(b), 8(c), and 8(d), one can observe the following.

(a) As mass 1.2 Kg was added into the base, little change in both T and TC can be observed.

(b) As damage happens, the peaks of T (5, 2), T (5, 3), as well as TC (5, 2), TC (5, 3), shift to the left direction; that is, the corresponding frequencies decrease, which confirm the simulation results described before. This observation suggests that the peak frequency shift can be used for detecting damage. Herein one needs to bear in mind that the T or TC should be well chosen.

(c) Apparently, T (5, 2) performs better than T (5, 3) in differentiating the difference in damage. The same conclusion can be drawn with TC, where TC (5, 2) is better than TC (5, 3) in distinguishing the difference in damage.

(d) Apart from this, one can observe that, during the experiment, the noise has a very small influence, as the coherence is close to value "1" in most parts. This also can be found in the transmissibility as T (5, 3) and T (5, 2) lines are very smooth. This observation on the TC is very important, which suggests that it can be used for checking whether the experiment is well conducted.

5.1.2. FRF Coherence and TC Comparison. In modal analysis, especially in experimental modal analysis, the excitation is acquired during the experiment process; and the FRF is a very important estimator for analyzing the structural dynamics characteristics. Herein, the FRF coherence (5, 1) is plotted in Figure 9 for the same state conditions as in the last subsection.

From Figure 9, one can also find the peak shifts between [60, 80] Hz. Additionally, comparing Figure 9 with TC (5, 3) in Figure 8(c) and TC (5, 2) in Figure 8(d), it can be observed that TC (5, 2) performs better than FRF coherence (5, 1) in differentiating differences in damage as the peaks of TC (5, 2) are more pronounced. However, if only concerning peak frequency shift, FRF coherence (5, 1) performs better than TC (5, 3) in Figure 8(c). Therefore, one can conclude that both TC and FRF coherence might be used for detecting damage via the peak frequency shift.

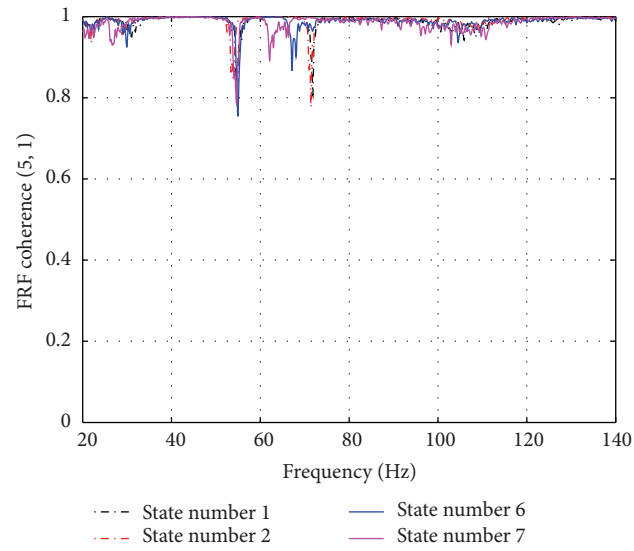

Figure 9: FRF coherence (5, 1) of measurement 1 of State numbers 1, 2, 6, and 7.

In order to better indicate the damage detection ability of transmissibility, TC, and FRF coherence, Table 4 shows the peak amplitude decrease and frequency shifts of the two obvious peaks in transmissibility, TC, and FRF coherence. From Table 4, one can find, from T (5, 2), TC (5, 2), and FRFC (5, 1), that all can perform well in damage detection with peak frequency shift and amplitude change. However, the second peak frequency change is higher than the first one, while the first peak amplitude changes more than the second one, with exception of TC (5, 2) in State #7.

Note that in real engineering, especially in operational modal analysis, normally the excitation cannot be measured.

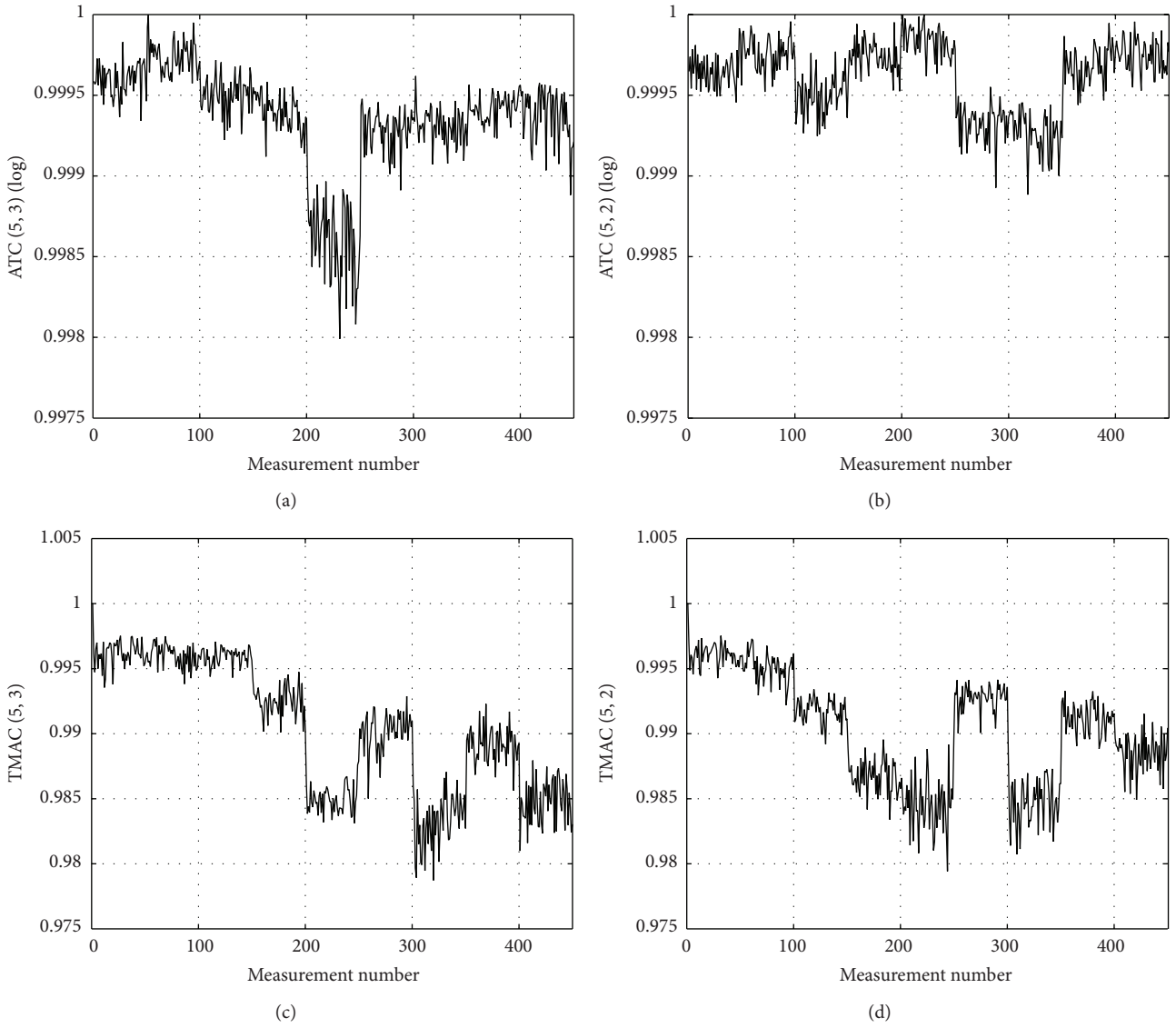

Figure 10: (a) ATC (5, 3), (b) ATC (5, 2), (c) TMAC (5, 3), and (d) TMAC (5, 2) for State numbers 1 to 9.

Thus, the FRF would be impossible to be used for modal analysis. Therefore, the TC will perform in its perfect way, as transmissibility is only depending on the structural responses, as well as TC.

5.2. Damage Identification Analysis in Linear Part. Damage detection plays a vital role in real-time SHM. As shown in Figures 8(c) and 8(d), TC might be used for detecting damage. Herein, ATC (5, 3) and ATC (5, 2) as well as TMAC (5, 3) and TMAC (5, 2) are shown in Figures 10(a), 10(b), 10(c), and 10(d), respectively, for 50 measurements from each of the nine state conditions (State numbers 1 to 9), with 450 measurements in total.

From a general perspective, one can observe that in both cases, ATC (ATC (5, 2), ATC (5, 3)) and TMAC (TMAC (5, 2) and TMAC (5, 3)), the variability is relatively small comparing with the reference value of unit, which suggests that these two indicators do not perform very well in detecting damage.

In Figures 10(a) and 10(b), for the mass type damage, that is, from D0 to D1 and D2, ATC (5, 3) and ATC (5, 2) increase when mass is added into the base structure, and when the mass is moved into the first floor, both ATC (5, 3) and ATC (5, 2) decrease. In this case, it would be hard to draw out a conclusion of mass influence into the indicator ATC. For stiffness reduction type damage, it is difficult to predict the presence of damage since ATC (5, 2) of State #5 is higher than the ones from the baseline State #1. However, in the case of ATC (5, 3), one might draw a conclusion that ATC (5, 3) can be used for detecting damage related to stiffness reduction as to all the measurements from State numbers 4–9, the corresponding ATC (5, 3) are lower than the baseline. Another aspect is that ATC (5, 3) might be also used to relatively quantify the damage as it varies proportionally to each state. One can also observe that, for each state, the values of 50 measurements vary not too much, which suggests that the experiment is conducted in a good condition.

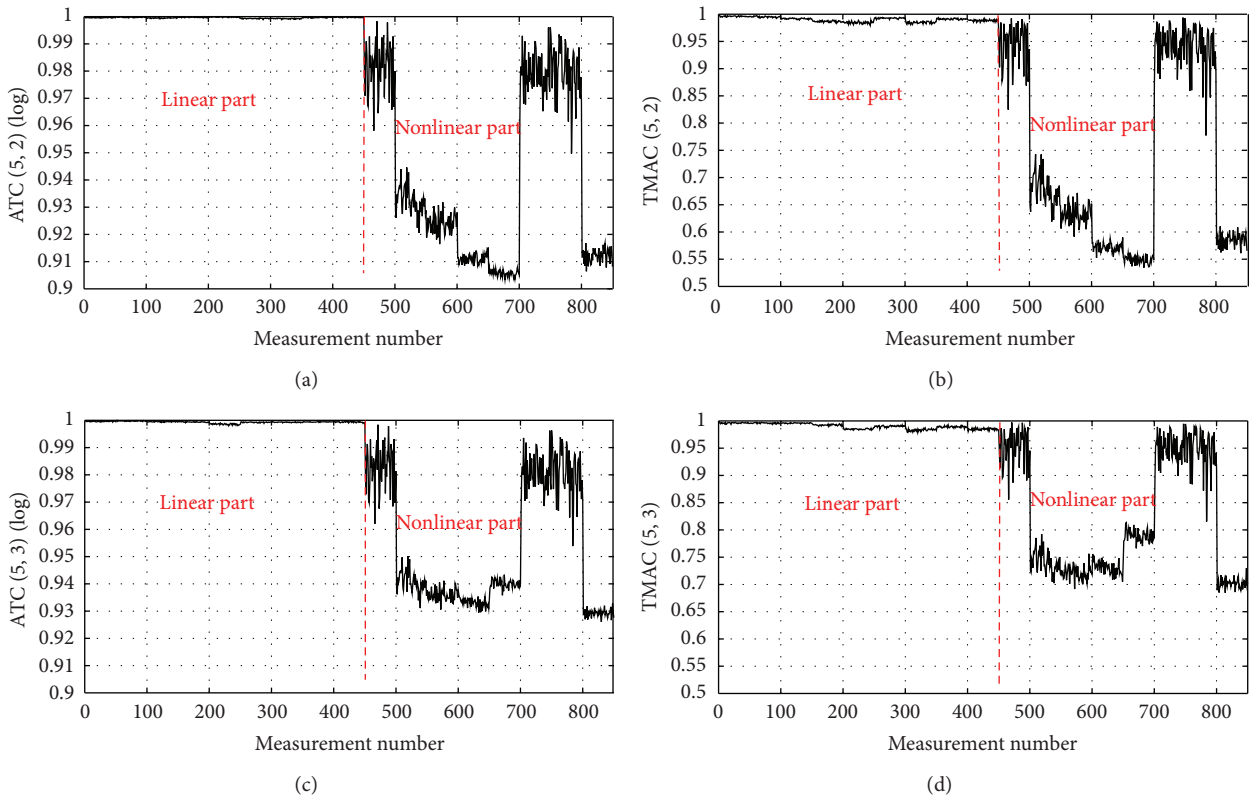

Figure 11: (a) ATC (5, 2), (b) TMAC (5, 2), (c) ATC (5, 3), and (d) TMAC (5, 3) for State numbers 1 to 17.

In Figures 10(c) and 10(d), for the mass adding damage type, it is clear that from State #1 to State #3, the TMAC (5, 3) and TMAC (5, 2) decreased as the mass 1.2 Kg was added into the base in State #2 and later moved to first floor in State #3. For stiffness reduction from State numbers 4 to 9, one can find that both TMAC (5, 3) and TMAC (5, 2) decrease as the stiffness reduction increased from State numbers 4 to 5, from State numbers 6 to 7, and from State numbers 8 to 9, respectively. In Figure 10(c), one can also observe that TMAC (5, 3) decreased clearly as the stiffness reduction changed from the first story to the second story and from second story to third story. Comparing State numbers 6 and 8, one can see some decrease occurring in TMAC (5, 3). For TMAC (5, 2), in Figure 10(d), it can be found that the TMAC (5, 2) decreases from State numbers 4 to 5, from State numbers 6 to 7, and from State numbers 8 to 9, meaning that the TMAC (5, 2) can relatively quantify the damage for each story. Comparing Figures 10(c) and 10(d), one might conclude that TMAC can be used for relatively quantifying damage. Note that this also confirms the same conclusion drawn out in the simulation section analysis.

5.3. Damage Identification Analysis in Nonlinear Part. In order to show the capacity of the proposed approach to detect nonlinear behaviours related to damage, Figure 11 shows the ATC (5, 2) and TMAC (5, 2) as well as ATC (5, 3) and TMAC (5, 3), respectively, for all 17 states. From the figure, one can clearly find that both damage-sensitive indicators, ATC and TMAC, perform much better in the nonlinear part (State numbers 10–17, 451–900) than in linear one (State numbers 1–9, 1–450). In the nonlinear part, one can see clearly that each state has been identified as outliers; that is, the ATC and TMAC successfully detect and identify the damage states.

6. Conclusions

This study illustrated the coherence between two outputs and newly defined TC, that is, transmissibility coherence; it built the relation between the TC and the traditional FRF coherence in modal analysis, following the construction of a damage-sensitive indicator using the modal assurance criterion, for detecting and relatively quantifying structural damage.

The TC has an important advantage over the FRF coherence, as the former does not need to know the input excitation to the system, which might be an important feature for real-world applications. The TC can be used for checking whether the experiment is well conducted, as it gives indications about the presence of noise in the system. It may also be used for detecting damage using the frequency shift as damage indicator. Additionally, the proposed ATC might be used for detecting damage especially in nonlinear analysis; it was demonstrated that in nonlinear damage quantification it performs well. In addition, the TC and related indicators are sensitive to environment variety like noise, which might be used for monitoring the operational conditions.

The TMAC can be used to relatively quantify the damage. The results of both the simulated frame and three-story frame

structure reveal the well performance in damage detection and quantification both in linear and in nonlinear part; in the linear part, all the damage scenarios were successfully detected and relatively well quantified; it was also demonstrated that, in the nonlinear part, the approach performs much better than in linear part.

It is important to note that the proposed approach only requires minimum two-sensor data acquisition in the structural system for detecting and relatively quantifying the structural damage. Therefore, it shows promising future in real time SHM.

Finally, for cases, simulation and experiment, the well performance in detecting and quantifying the damage shows great promising future in real engineering usage.

Conflict of Interests

The authors declare that there is no conflict of interests regarding the publication of this paper.

Acknowledgments

The writers acknowledge the support for the work reported in this paper from the Spanish Ministry of Economy and Competitiveness (Project no. BIA2013-46944-C2-1-P). Financial support for the CSC research fellowship given to Yun-Lai Zhou is also acknowledged. The coauthor N. Maia would like to acknowledge the support of the Portuguese Science Foundation FCT, through IDMEC, under LAETA.

References

[1] E. Figueiredo, I. Moldovan, and M. B. Marques, *Condition Assessment of Bridges: Past, Present, and Future. A Complementary Approach*, Universidade Católica Editora, 2013.

[2] H. Sohn, C. R. Farrar, F. M. Hemez, D. D. Shunk, D. W. Stinemates, and B. R. Nadler, *A Review of Structural Health Monitoring Literature: 1996–2001*, Los Alamos National Laboratory, Los Alamos, NM, USA, 2003.

[3] D. Montalvão, N. M. M. Maia, and A. M. R. Ribeiro, "A review of vibration-based structural health monitoring with special emphasis on composite materials," *Shock and Vibration Digest*, vol. 38, no. 4, pp. 295–324, 2006.

[4] W. Weijtjens, G. De Sitter, C. Devriendt, and P. Guillaume, "Relative scaling of mode shapes using transmissibility functions," *Mechanical Systems and Signal Processing*, vol. 40, no. 1, pp. 269–277, 2013.

[5] N. M. M. Maia, R. A. B. Almeida, A. P. V. Urgueira, and R. P. C. Sampaio, "Damage detection and quantification using transmissibility," *Mechanical Systems and Signal Processing*, vol. 25, no. 7, pp. 2475–2483, 2011.

[6] Z. Mao and M. Todd, "A model for quantifying uncertainty in the estimation of noise-contaminated measurements of transmissibility," *Mechanical Systems and Signal Processing*, vol. 28, pp. 470–481, 2012.

[7] Y. E. Lage, N. M. M. Maia, and M. M. Neves, "Force magnitude reconstruction using the force transmissibility concept," *Shock and Vibration*, vol. 2014, Article ID 905912, 9 pages, 2014.

[8] W. Heylen, S. Lammens, and P. Sas, *Modal Analysis Theory and Testing*, section A.6, K.U. Leuven-PMA, Brussels, Belgium, 1998.

[9] R. P. C. Sampaio and N. M. M. Maia, "Strategies for an efficient indicator of structural damage," *Mechanical Systems and Signal Processing*, vol. 23, no. 6, pp. 1855–1869, 2009.

[10] A. S. Gevins, "Overview of computer analysis," in *Handbook of Electroencephalography and Clinical Neurophysiology*, A. S. Gevins and A. Remond, Eds., vol. 1, pp. 31–83, Elsevier, New York, NY, USA, 1987.

[11] M. A. Guevara, I. Lorenzo, C. Arce, J. Ramos, and M. Corsi-Cabrera, "Inter- and intrahemispheric EEG correlation during sleep and wakefulness," *Sleep*, vol. 18, no. 4, pp. 257–265, 1995.

[12] T. L. Paez, "The history of random vibrations through 1958," *Mechanical Systems and Signal Processing*, vol. 20, no. 8, pp. 1783–1818, 2006.

[13] E. A. Robinson, "A historical perspective of spectrum estimation," *Proceedings of the IEEE*, vol. 70, no. 9, pp. 885–907, 1982.

[14] J. Kopal, O. Vyšata, J. Burian, M. Schätz, A. Procházka, and M. Vališ, "Complex continuous wavelet coherence for EEG microstates detection in insight and calm meditation," *Consciousness and Cognition*, vol. 30, pp. 13–23, 2014.

[15] R. Srinivasan, W. R. Winter, J. Ding, and P. L. Nunez, "EEG and MEG coherence: measures of functional connectivity at distinct spatial scales of neocortical dynamics," *Journal of Neuroscience Methods*, vol. 166, no. 1, pp. 41–52, 2007.

[16] V. Sakkalis and M. Zervakis, "Linear and nonlinear synchronization analysis and visualization during altered states of consciousness," in *Recent Advances in Biomedical Engineering*, chapter 25, pp. 493–517, InTech, 2009.

[17] A. V. Tankanag, A. A. Grinevich, T. V. Kirilina, G. V. Krasnikov, G. M. Piskunova, and N. K. Chemeris, "Wavelet phase coherence analysis of the skin blood flow oscillations in human," *Microvascular Research*, vol. 95, pp. 53–59, 2014.

[18] J. S. Schuman, M. R. Hee, C. A. Puliafito et al., "Quantification of nerve fiber layer thickness in normal and glaucomatous eyes using optical coherence tomography: a pilot study," *Archives of Ophthalmology*, vol. 113, no. 5, pp. 586–596, 1995.

[19] J.-S. Hu and M.-T. Lee, "Multi-channel post-filtering based on spatial coherence measure," *Signal Processing*, vol. 105, pp. 338–349, 2014.

[20] J.-S. Lew, "Using transfer function parameter changes for damage detection of structures," *AIAA Journal*, vol. 33, no. 11, pp. 2189–2193, 1995.

[21] J. E. Michaels and T. E. Michaels, "Detection of structural damage from the local temporal coherence of diffuse ultrasonic signals," *IEEE Transactions on Ultrasonics, Ferroelectrics, and Frequency Control*, vol. 52, no. 10, pp. 1769–1782, 2005.

[22] D. D. Rizos, S. D. Fassois, Z. P. Marioli-Riga, and A. N. Karanika, "Vibration-based skin damage statistical detection and restoration assessment in a stiffened aircraft panel," *Mechanical Systems and Signal Processing*, vol. 22, no. 2, pp. 315–337, 2008.

[23] D. D. Rizos, S. D. Fassois, Z. P. Marioli-Riga, and A. N. Karanika, "Statistical skin damage detection and restoration assessment for aircraft panels via vibration testing," in *Proceedings of the 1st European Workshop on Structural Health Monitoring*, pp. 1211–1218, Paris, France, 2002.

[24] S. D. Fassois and J. S. Sakellariou, "Time-series methods for fault detection and identification in vibrating structures," *Philosophical Transactions of the Royal Society of London, Series A: Mathematical, Physical and Engineering Sciences*, vol. 365, no. 1851, pp. 411–448, 2007.

[25] G. R. Cooper and C. D. McGillem, *Probabilistic Methods of Signal and System Analysis*, Holt, Rinehart, and Winston, New York, NY, USA, 1971.

[26] E. Figueiredo, L. Radu, K. Worden, and C. R. Farrar, "A Bayesian approach based on a Markov-chain Monte Carlo method for damage detection under unknown sources of variability," *Engineering Structures*, vol. 80, pp. 1–10, 2014.

[27] E. Figueiredo, G. Park, C. R. Farrar, K. Worden, and J. Figueiras, "Machine learning algorithms for damage detection under operational and environmental variability," *International Journal of Structural Health Monitoring*, vol. 10, no. 6, pp. 559–572, 2011.

[28] M. B. Priestley, *Spectral Analysis and Time Series*, Academic Press, New York, NY, USA, 1981.

[29] V. Sakkalis and M. Zervakis, "Linear and nonlinear synchronization analysis and visualization during altered states of consciousness," in *Recent Advances in Biomedical Engineering*, G. R. Naik, Ed., chapter 25, InTech, 2009.

[30] http://es.mathworks.com/help/signal/ug/cross-spectrum-and-magnitude-squared-coherence.html.

[31] C. Zheng, M. Zhou, and X. Li, "On the relationship of non-parametric methods for coherence function estimation," *Signal Processing*, vol. 88, no. 11, pp. 2863–2867, 2008.

[32] C. J. Schallhorn, *Localization of vibration-based damage detection method in structural applications [M.S. thesis]*, University of Iowa, 2012.

[33] N. M. M. Maia and J. M. M. Silva, *Theoretical and Experimental Modal Analysis*, vol. 8 of *Mechanical Engineering Research Studies: Engineering Dynamics*, Research Studies Press, 2003.

[34] R. Bortel and P. Sovka, "Statistical evaluation of coherence estimated from optimally beamformed signals," *Computers in Biology and Medicine*, vol. 43, no. 9, pp. 1286–1262, 2013.

[35] P. D. Welch, "The use of fast Fourier transform for the estimation of power spectra: a method based on time averaging over short, modified periodograms," *IEEE Transactions on Audio and Electroacoustics*, vol. 15, no. 2, pp. 70–73, 1967.

[36] J. Capon, "High resolution frequency-wavenumber spectrum analysis," *Proceedings of the IEEE*, vol. 57, no. 8, pp. 1408–1418, 1969.

[37] R. J. Allemang and D. L. Brown, "A correlation coefficient for modal vector analysis," in *Proceedings of the 1st International Modal Analysis Conference & Exhibit*, pp. 110–116, 1982.

[38] R. Pascual, J. C. Golinval, and M. Razeto, "Frequency domain correlation technique for model correlation and updating," in *Proceedings of the 15th International Modal Analysis Conference (IMAC '97)*, pp. 587–592, February 1997.

[39] W. Heylen and P. Avitabile, "Correlation considerations—part 5 (degree of freedom correlation techniques)," in *Proceedings of the 16th International Modal Analysis Conference*, pp. 207–214, February 1998.

[40] E. Figueiredo, G. Park, J. Figueiras, C. Farrar, and K. Worden, "Structural health monitoring algorithm comparisons using standard data sets," Los Alamos National Laboratory Report LA-14393, Los Alamos National Laboratory, 2009.

[41] http://institute.lanl.gov/ei/structural-health-monitoring/test-structures-applications/.